



ELSEVIER

Available online at www.sciencedirect.com

SCIENCE @ DIRECT®

EPSL

Earth and Planetary Science Letters 222 (2004) 583–597

www.elsevier.com/locate/epsl

$^{40}\text{Ar}/^{39}\text{Ar}$ ages of tephras intercalated in astronomically tuned Neogene sedimentary sequences in the eastern Mediterranean[☆]

K.F. Kuiper^{a,b,*}, F.J. Hilgen^a, J. Steenbrink^c, J.R. Wijbrans^b

^aIPPU, Utrecht University, Budapestlaan 4, 3584 CD Utrecht, The Netherlands

^bDepartment of Isotope Geochemistry, Vrije Universiteit Amsterdam, De Boelelaan 1085, 1081 HV Amsterdam, The Netherlands

^cNederlandse Aardolie Maatschappij (NAM), Postbus 28000, 9400 HH Assen, The Netherlands

Received 18 June 2003; received in revised form 2 March 2004; accepted 4 March 2004

Abstract

We present new $^{40}\text{Ar}/^{39}\text{Ar}$ data for sanidine and biotite derived from volcanic ash layers that are intercalated in Pliocene and late Miocene astronomically dated sequences in the Mediterranean with the aim to solve existing inconsistencies in the intercalibration between the two independent absolute dating methods. $^{40}\text{Ar}/^{39}\text{Ar}$ sanidine ages are systematically younger by 0.7–2.3% than the astronomical ages for the same ash layers. The significance of the discrepancy disappears except for the upper Ptolemais ashes, which reveal the largest difference, if an improved full error propagation method is applied to calculate the absolute error in the $^{40}\text{Ar}/^{39}\text{Ar}$ ages. The total variance is dominated by that of the activity of the decay of ^{40}K to ^{40}Ar (~ 70%) and that the amount of radiogenic $^{40}\text{Ar}_p$ in the primary standard GA1550 biotite (~ 15%). If the $^{40}\text{Ar}/^{39}\text{Ar}$ ages are calculated relative to an astronomically dated standard, the influence of these parameters is greatly reduced, resulting in a more reliable age and in a significant reduction of the error in $^{40}\text{Ar}/^{39}\text{Ar}$ dating.

Astronomically calibrated ages for Taylor Creek Rhyolite (TCR) and Fish Canyon Tuff (FCT) sanidine are 28.53 ± 0.02 and 28.21 ± 0.04 Ma (± 1 S.E.), respectively, if we start from the more reliable results of the Cretan A1 ash layer. The most likely explanation for the large discrepancy found for the younger Ptolemais ash layers (equivalent to FCT of 28.61 Ma) is an error in the tuning of this part of the sequence.

© 2004 Elsevier B.V. All rights reserved.

Keywords: $^{40}\text{Ar}/^{39}\text{Ar}$ dating; Fish Canyon Tuff; cyclostratigraphy; astronomical time scale; orbital forcing; Neogene; Mediterranean

1. Introduction

$^{40}\text{Ar}/^{39}\text{Ar}$ dating is a versatile technique to determine the age of a variety of K-bearing minerals,

while astronomical dating is based on the correlation or tuning of cyclic variations in the stratigraphic record to computed time series of orbital variations. The latter provides a completely independent method to determine the absolute age and duration of geological processes. The calibration of the standard geological time scale depends on two independent absolute dating techniques, namely, astronomical tuning for the youngest Plio–Pleistocene part and radio-isotopic (e.g., $^{40}\text{Ar}/^{39}\text{Ar}$ dating)

[☆] Supplementary data associated with this article can be found, in the online version, at doi: 10.1016/j.epsl.2004.03.005.

* Corresponding author. IPPU, Utrecht University, Budapestlaan 4, 3584 CD Utrecht, The Netherlands. Tel.: +31-30-253-5418; fax: +31-30-253-1677.

E-mail address: kkuiper@geo.uu.nl (K.F. Kuiper).

for older parts of the time scale. A reliable intercalibration of these methods is urgently needed, also because the entire Neogene will rely on astronomical dating in the next version of the standard time scale [1].

In a first attempt, Renne et al. [2] compared $^{40}\text{Ar}/^{39}\text{Ar}$ ages of seven geomagnetic polarity transitions over the last 3.4 Ma, with astronomical ages assigned to the same polarity transitions but in other sections. The disadvantage of this method is the required interpolation of the sedimentation rate between the stratigraphic positions of isotopically dated volcanic material to obtain the age of the reversal in the same section for five of the studied reversals. Furthermore, the magnetostratigraphy of both the astronomically tuned sections and the sections containing the $^{40}\text{Ar}/^{39}\text{Ar}$ dated material must be reliable.

Therefore, $^{40}\text{Ar}/^{39}\text{Ar}$ experiments were performed on K-bearing minerals derived from tephra layers intercalated in astronomically tuned sedimentary sequences. In this way, astronomical ages can be assigned to a tephra layer, and both methods are directly compared. Hilgen et al. [3] reported the first $^{40}\text{Ar}/^{39}\text{Ar}$ ages of Miocene tephra from astronomically tuned marine sections on Crete and concluded that the $^{40}\text{Ar}/^{39}\text{Ar}$ ages were not significantly different from the astronomical ages. But Steenbrink et al. [4] subsequently published discrepancies between $^{40}\text{Ar}/^{39}\text{Ar}$ ages for a series of Pliocene tephra intercalated in the astronomically tuned sediments of the lacustrine Ptolemais basin, the $^{40}\text{Ar}/^{39}\text{Ar}$ ages being significantly younger by $\sim 3\text{--}4\%$. In an attempt to unravel the cause of the different outcome of these studies, we decided to perform a new series of experiments. The data of these experiments on the ash layers in the lacustrine Ptolemais succession in NW Greece and in the slightly older marine succession on Crete are presented in this paper.

2. Geological setting and sections

Part of the ash layers studied here originate from Tortonian to Messinian deep marine sediments exposed on the eastern part of the island of Crete (southern Greece) and the island of Gavdos (Metochia

section), immediately south of Crete (Fig. 1). The sections on Crete consist of a cyclic alternation of whitish, indurated, carbonate-rich marls and grey, carbonate-poor marls (lower part Faneromeni section) or of homogeneous marls and sapropels; the latter are intercalated in, or substitute, the grey carbonate-poor beds (Faneromeni upper part, Kastelli, Agios Ioannis and Metochia). The upper part of the Metochia section is characterized by cyclically bedded diatomites. The volcanic source of the ash layers in these Miocene sequences is unclear.

The Pliocene volcanic ash layers are intercalated in the lacustrine Ptolemais Formation, the middle of three lithostratigraphic units forming the basin fill of the Pliocene Ptolemais basin in northern Greece (Fig. 1). The $\sim 110\text{-m}$ -thick Ptolemais Formation consists of bipartite cycles of alternating grey or beige colored marls and lignites [5]. Volcanic ash layers are intercalated in the lignite and marl beds of the Ptolemais Formation. The volcanic source of the ash layers is most likely to be found in the Edessa area or Voras Mountains located nearby [6,7].

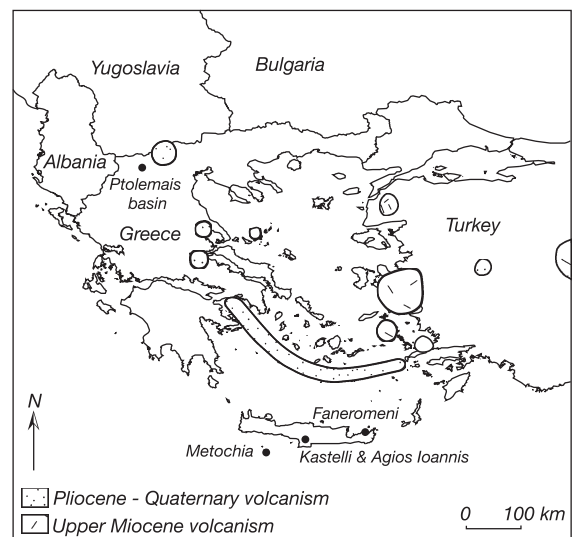


Fig. 1. Locations of the studied sections. The A1 ash is found in several sections on Crete and Gavdos. The A1 sanidine and biotite dated in this study come from the Faneromeni, Kastelli and Agios Ioannis sections. The distribution of Neogene volcanism in this area is highlighted, indicating possible sources of the studied volcanic ash layers (based on [29]).

3. Astronomical time control for the volcanic ash layers

Hilgen et al. [3,9] and Krijgsman et al. [8] described the astrochronological tuning for the volcanic ash layers on Crete in detail. The astronomical ages for the volcanic ash layers in the Ptolemais basin are based on [4,10]. A brief summary of the astrochronological tuning is given here.

Fig. 2 shows the astronomical tuning of the marine sections on Crete to the 65°N summer insolation curve of solution La93 [11], where each sapropel/grey marl is numbered as in [9]. Because the cycle patterns for these Miocene sections are similar to the patterns in the Mediterranean Plio–Pleistocene (e.g., [12]), the same phase relations were used for the tuning. The tuning of Agios Ioannis and Kastelli sections is less straightforward and was achieved using detailed

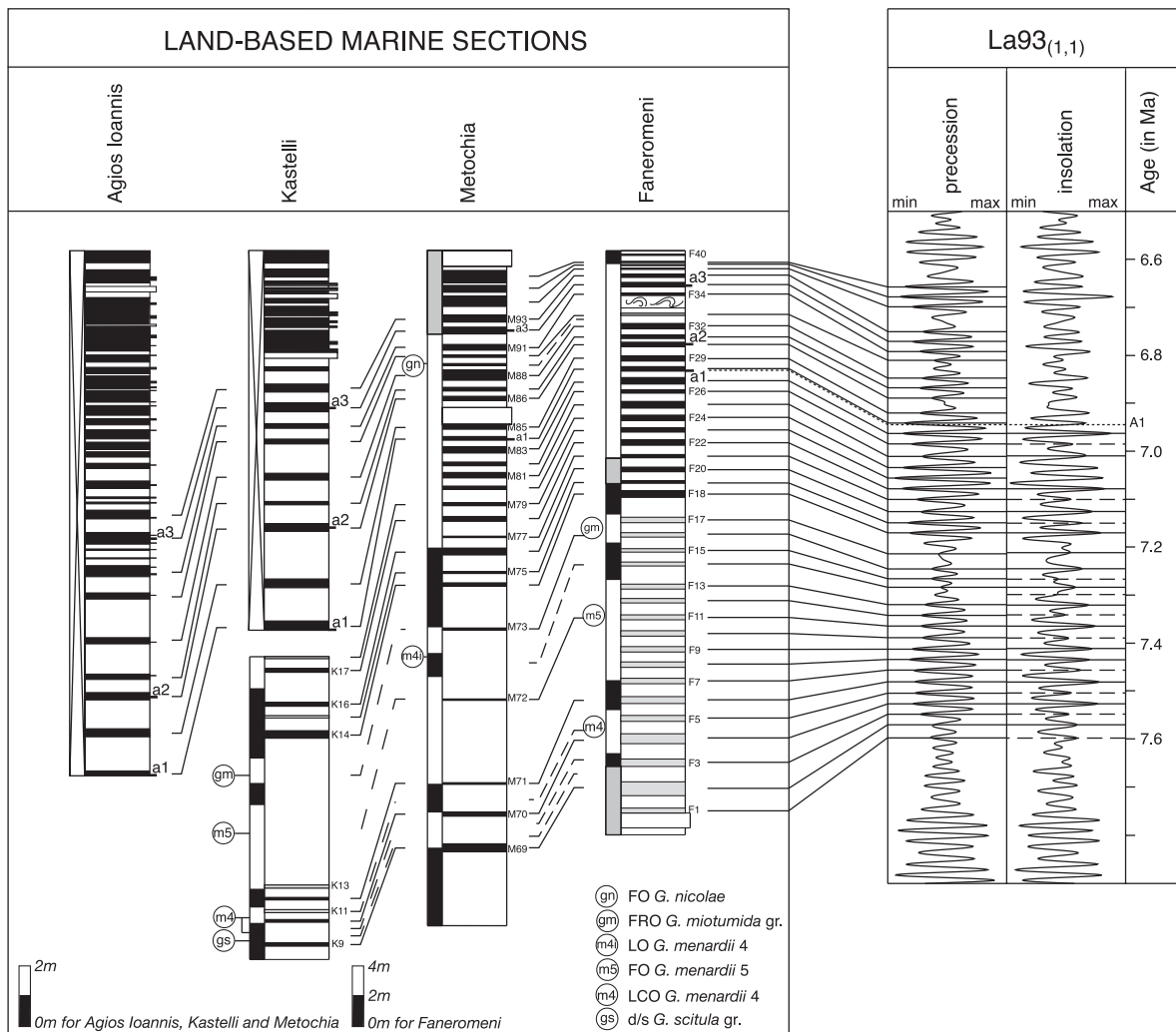


Fig. 2. Astronomical tuning of the Agios Ioannis, Kastelli, Metochia and Faneromeni sections to the 65°N summer insolation curve of solution La93_(1,1) [11] with present day values for the dynamical ellipticity and tidal dissipation (after [3,9]). The individual sapropels correspond to precession minima, small-scale sapropel clusters (consisting of three or four sapropels) correspond to 100 kyr eccentricity maxima and large-scale sapropel clusters (containing three or four small-scale clusters) correspond to 400 kyr eccentricity maxima.

cyclostratigraphic and biostratigraphic correlations [3].

Fig. 3 shows the tuning of the sedimentary cycles in the Ptolemais basin to the 65°N summer insolation curve of La93 as described in detail by

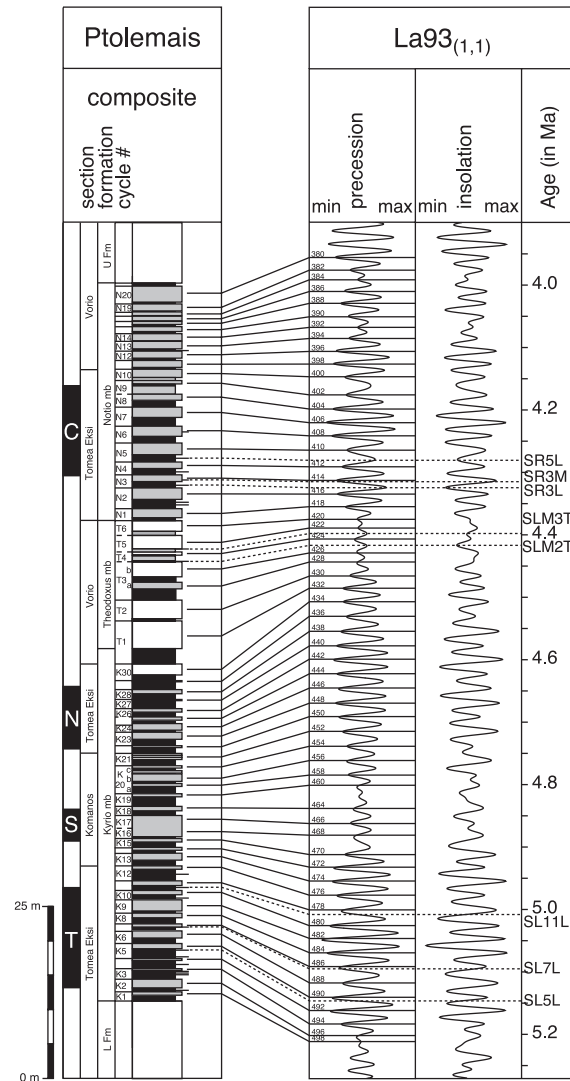


Fig. 3. Astronomical tuning of the Ptolemais section to the 65°N summer insolation curve of solution La93_(1,1) [11] with present day values for the dynamical ellipticity and tidal dissipation showing the tuning of [10] without a hiatus between K18 and K19. The two different tuning options as described in [10] might slightly change the astronomical ages of the volcanic ash layers SLM2T and SLM3T.

[4,10]. Due to the lack of a clear expression of eccentricity, the magnetostratigraphy of the Ptolemais composite was calibrated to the APTS [13] for a first-order age control. Ages of the corresponding reversals in the APTS served as a starting point for the tuning of the lignite–marl cycles as presented in Fig. 3.

Van Vugt et al. [10] mentioned field evidence for a hiatus between cycles K18 and K19, where a shallow scouring surface pointed to erosion while the thin paleosol on top of the surface was interpreted as a period of non-deposition. Therefore, tuning of the cycles K19 to T6 is less straightforward and resulted in two options, one supporting a hiatus of three cycles and one without a hiatus. However, this uncertainty is assumed to affect the ages of the ash layers SLM2T and SLM3T only (Fig. 3).

4. Materials and methods

4.1. Material

On Crete and in the Ptolemais basin volcanic ash levels were collected at several localities. Exact locations of the sampled sections are given in [3] for the Cretan ashes and in [4] for Ptolemais. Most of the ash layers contain the K-rich minerals biotite and sanidine. On Crete, A3 and A1 showed mixed plagioclase/sanidine populations and A2 contained only plagioclase. In Ptolemais, all the dated ash layers contained a plagioclase/sanidine population, but it was relatively easy to separate a pure sanidine fraction. The biotite crystals in the Ptolemais ash layers have been partially altered to chlorite with the exception of biotite in ash layer SR3M. The bulk samples were crushed (depending on their solidity), washed and sieved. The maximum grain-size fraction of 400–500 μm or, when not available, smaller grain-size fractions of 250–400 μm and/or 125–250 μm were used for standard magnetic and heavy liquid separations of micas and sanidine. Subsequently, all samples were handpicked and cleaned in an ultrasonic bath with distilled water. Sanidine samples (SLM2T, SLM3T, SR3M, SR3L and A1) were divided into three splits, which were respectively leached with HF/HNO₃, HNO₃ or not leached, but no differences in ages due to leaching were found.

4.2. $^{40}\text{Ar}/^{39}\text{Ar}$ analytical procedure

The samples were wrapped in Al-foil and loaded in 6 mm ID quartz vials. Two different standards Fish Canyon Tuff sanidine (FCT obtained from H. Baadsgaard for irradiation VU32; FC-2 obtained from P.R. Renne for all other irradiations) and Taylor Creek Rhyolite (TCR) sanidine (85G003 for VU32 and VU37; TCR2a, a new split obtained from M. Pringle for VU37 and VU41) were wrapped in Cu-foil and loaded at top and bottom positions in the vial and between each set of 3–5 samples. Samples were irradiated in several batches (VU32, VU37 and VU41) in the Oregon State University TRIGA reactor in the cadmium shielded CLICIT facility for 7 h (VU32 and VU37). VU41 was also irradiated in the CLICIT facility but in a more central position in the reactor, so that the flux gradient over the length of the tube was less than that for the preceding irradiations. After irradiation, samples and standards were loaded in 2-mm diameter holes of a 60-mm diameter copper planchet and placed in an ultrahigh vacuum extraction line. Samples and standards were stepwise heated or directly fused, and gas was analyzed isotopically with a Mass Analyser Products LTD 215-50 noble gas mass spectrometer.

Multiple grain and, in a very few cases, single grains of sanidine of standards and samples were preheated using a defocused laser beam with an output of 2 W (samples did not glow and gas was pumped away) to remove undesirable atmospheric argon. After this preheating step, the samples and standards were analyzed by total fusion with a 24 W—continuous wave argon-ion—laser. Experiments were replicated 5–10 times for total fusion analyses. Multiple-grain fractions of biotite samples were measured by stepwise heating or fusion (preheating step with 0.2 W defocused laser beam). Most of the samples were included in several irradiations to check the reproducibility of the results. Beam intensities of Ar isotopes were measured in a peak-jumping mode at half-mass intervals over the 40–35.5 mass range on a secondary electron multiplier using switchable amplifier resistors with gains of 5×10^4 , 5×10^3 and 5×10^2 . For data collection, the mass spectrometer is operated with a modified version of standard MAP software (i.e., adjustable number of integration cycles per peak, amplifier range switching and valve con-

trol). System blanks were measured every three steps. The total system blanks were in the range of $1-10 \times 10^{-17}$ moles for mass 40, $1-5 \times 10^{-18}$ moles for mass 39, mass 38 and mass 36, and ca. $1-3 \times 10^{-17}$ moles for mass 37. Mass discrimination (1.002–1.0100 per atomic mass unit) was monitored by frequent analysis of $^{40}\text{Ar}/^{38}\text{Ar}$ reference gas or $^{40}\text{Ar}/^{36}\text{Ar}$ air pipette aliquots.

4.3. Age calculation

Regressions of the individual isotopes, blank corrections, corrections for nuclear interference reactions and mass discrimination corrections have been performed with the in-house developed ArArCalc (v2.20c) software [14]. The average value of blank analyses before and after measurement of an unknown is commonly applied as blank correction for all isotopes. When the contribution of different parameters to the variance (σ^2) in the $^{40}\text{Ar}^*/^{39}\text{Ar}_K$ ratio of an individual analysis is assessed, it appeared that ^{36}Ar blank values are contributing significantly to the variance. Therefore, ^{36}Ar blank corrections were studied in more detail and, depending on their (daily) behavior occasionally, a linear or polynomial fit of blank values over a certain (daily) period was applied for this isotope.

The analytical data are reported as weighted mean $^{40}\text{Ar}/^{39}\text{Ar}$ (or F) ratios with standard errors of the mean weighted with the inverse of the variance [15]. The data of replicate experiments from one irradiation package are combined, although this does not necessarily imply that all samples were analyzed within a single run. MSWD values in combination with a Student's t factor are used to assess the homogeneity in a sample or underestimation of analytical errors [16]. The analytical uncertainty in the F ratio of a sample is multiplied by $\sqrt{\text{MSWD}}$, when $\text{MSWD} > 1$. $\text{MSWD}'s > 1$ are in all cases (except VU32-C16 and VU37-C52) higher than the Student's t factor. When combining data with different J values (i.e., from different irradiation positions), the F ratios of the unknowns are divided by the F ratios of the standard (TCR in VU32, VU37 and older irradiations) and combined to a weighted mean in intercalibration factor $R_{\text{TC}}^{\text{Ash}}$ with a standard error of the mean. For irradiation, VU41 with FCT as main

standard $R_{TC}^{Ash} = R_{FC}^{Ash} \times R_{TC}^{FC}$ is used to establish the weighted mean intercalibration factor with a R_{TC}^{FC} of 1.0112 ± 0.0010 [17], confirmed in [18].

Ages and uncertainties have been calculated according to standard age equations using the consensus decay constants of [19] and an absolute age of $28.34 \pm 0.16/28.02 \pm 0.16$ Ma (or ± 0.28 Ma when decay constant errors are included) for TCR/FCT [17]. Uncertainties are reported at three levels. The first level includes the analytical uncertainty in the sample and the standard (Table A1, I); the second level includes the uncertainty in the absolute age of the standard (Table A1, II); and the third level adds the uncertainty in the decay constants as reported in [19] (σ_λ is $0.01 \times 10^{-10} \text{ yr}^{-1}$; Table A1, III). All errors are quoted at the 1σ significance level.

We used a slightly modified equation of [20] to determine absolute $^{40}\text{Ar}/^{39}\text{Ar}$ ages with most realistic error estimates [Eqs. (1) and (2); Appendix A] relative to one or more secondary standards intercalibrated to primary standard GA1550. Recently, Spell and McDougall [21] compiled potassium data for GA1550 over a period from 1968 to 2001 resulting in a potassium content of 7.646 ± 0.006 wt.%. Additionally, they established an intercalibration factor R_{GA1550}^{FC} of 0.2797 ± 0.0004 resulting in age for FCT of 28.10 ± 0.04 Ma. However, the uncertainty in [21] of ± 0.04 Ma includes only the analytical uncertainties in the $^{40}\text{Ar}^*/^{39}\text{Ar}_K$ ratios of GA1550 and FC, and this will increase when uncertainties in the absolute $^{40}\text{Ar}^*$ and ^{40}K contents in the primary standards and decay constants are incorporated. For the moment, we decided to use the commonly applied FCT age of 28.02 Ma based on data of [17] to avoid further confusion about absolute ages of standards.

5. Results

In Table A1, the analytical data are given for all experiments (more extended data tables can be found on <http://www.geo.vu.nl/users/kuik>). When the age and error was estimated according to Eqs. (1) and (2) (last column in Table A1; Appendix A), it appeared that, for all analyses, the variance (σ^2) is dominated by the uncertainty in the activity of the ^{40}K decay to

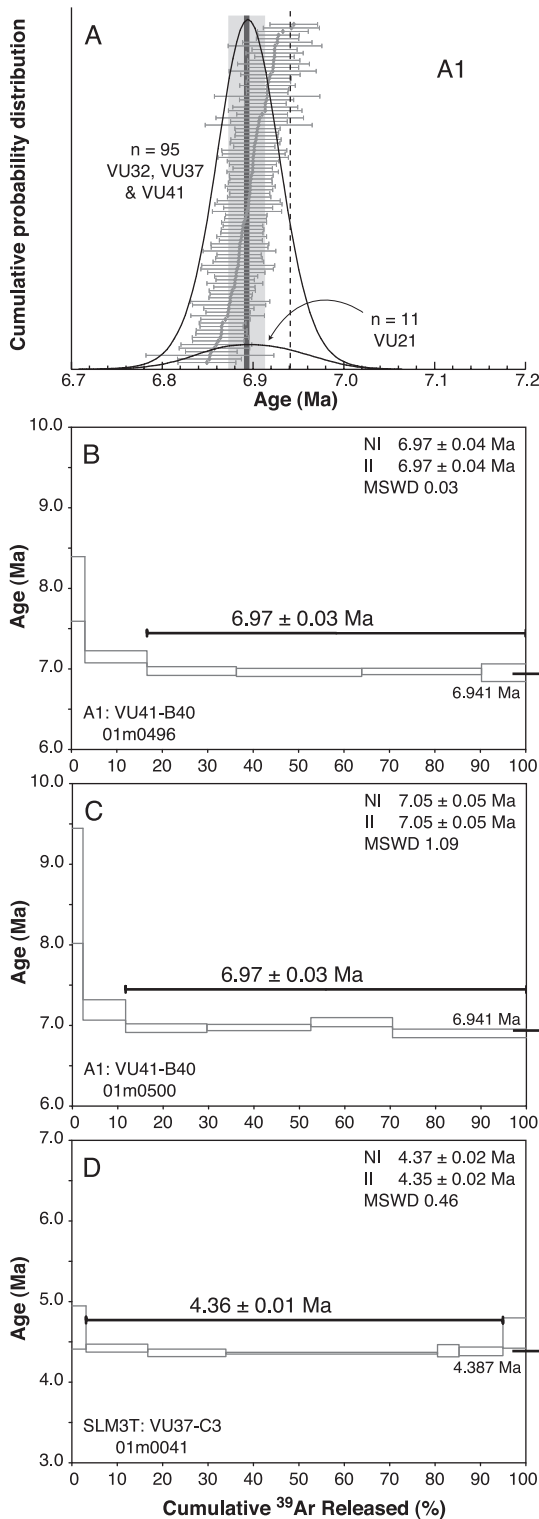
^{40}Ar ($\sim 70\%$) and the uncertainty in the radiogenic ^{40}Ar content in the primary standard ($\sim 15\%$). $^{40}\text{Ar}/^{39}\text{Ar}$ age probability distributions are shown in Figs. 4 and 5, where the vertical dashed lines represent astronomical ages of each volcanic ash layer; incremental heating spectra for the biotite analyses are shown in Fig. 4. No reliable $^{40}\text{Ar}/^{39}\text{Ar}$ ages were obtained for ash layers A2 and A3 on Crete because of very low ^{40}Ar intensities introducing large analytical errors measured on plagioclase, lack of reliable isochrons and MSWD's >1 , indicating heterogeneity.

5.1. Crete A1 sanidine

On Crete, the ash layer A1 is the most prominent of the three and was identified in several sections in different parts of Crete. This ash layer has been dated several times in six different irradiations with sample splits obtained during a number of field campaigns and from various locations and using different mineral separations and mineral treatment techniques (HF-leaching, no leaching). Hilgen et al. [3] already published some A1 data. The new experimental data on sanidine of irradiation packages from VU32, VU37 and VU41 are listed in Table A1. MSWD's are near or smaller than 1. When all R_{TC}^{A1} for individual experiments are combined to a weighted mean R_{TC}^{A1} , the MSWD is 0.53 (with $n=95$). Furthermore, isochron intercepts do not deviate from an atmospheric $^{40}\text{Ar}/^{36}\text{Ar}$ intercept of 295.5 at the 95% confidence level. The $^{40}\text{Ar}/^{39}\text{Ar}$ age for the A1 sanidine based on 95 individual analyses from several locations on Crete in several irradiation batches is the weighted mean age of 6.893 ± 0.093 Ma [1σ according to Eq. (2) in Appendix A, where F_u/F_{TC} first is combined to a weighted mean intercalibration factor R_{TC}^{A1} with standard error $\sigma_{R_{TC}^{A1}}$].

5.2. Crete A1 biotite

In VU32, incremental heating and total fusion experiments, and, in VU41, incremental heating experiments have been performed on biotite of Faneromeni A1. We were not able to deduce a reliable age spectrum in VU32, but we were able to reproduce two age spectra in VU41 (Fig. 4). The combined age of the



two spectra is 6.967 ± 0.096 Ma (Table A1). The first steps were omitted from the plateau according to criteria for a reliable plateau as defined by, e.g., [22]. Isochron intercepts did not differ from the atmospheric ratio at 95% confidence level.

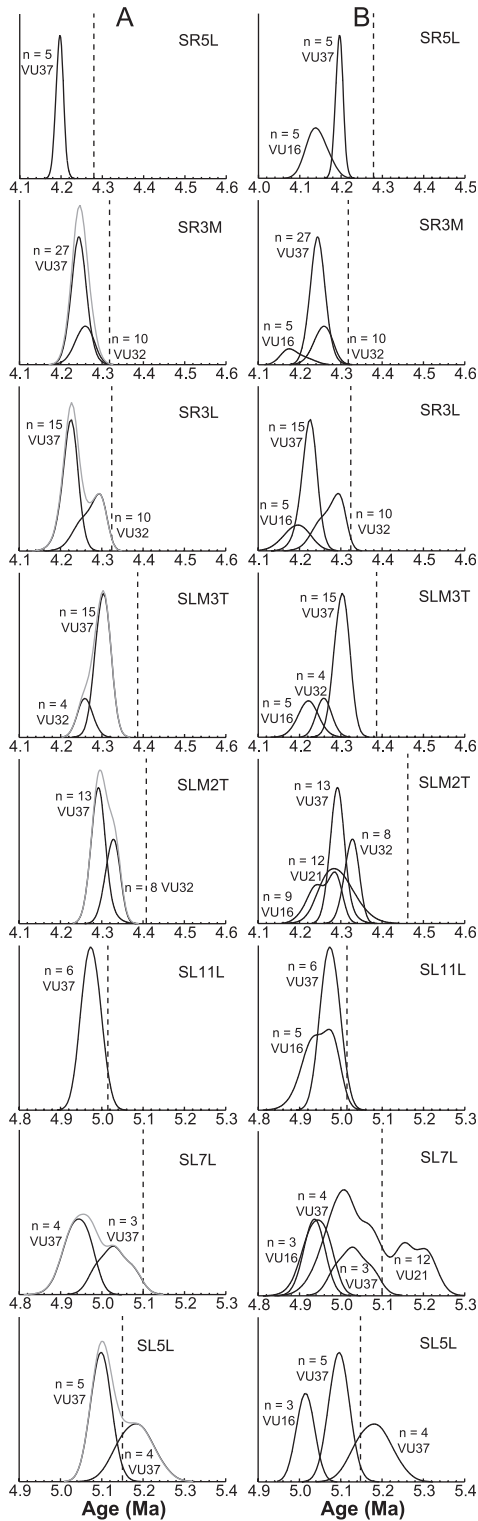
5.3. Ptolemais

Steenbrink et al. [4] already showed that sanidine from the Ptolemais tephra displayed straightforward incremental heating spectra where only the first and last steps were occasionally omitted because of the large uncertainties (those steps were never statistically different from the mean age of the age spectrum). Therefore, we only performed total fusion experiments after a preheating step to increase the number of analyses and to decrease the amount of material required for analysis. Furthermore, the seven isotopically dated ash layers in Ptolemais will be regarded as two groups: the older ashes SL5L, SL7L and SL11L, and the younger ashes SLM2T, SLM3T, SR3L, SR3M and SR5L, because they are intercalated in different parts of the succession separated by a possible hiatus.

5.4. The older Ptolemais ash layers

The analytical details and ages for the three ash layers are presented in Table A1. Measurements on the oldest ash layer in Ptolemais (SL5L) appeared to be on sanidine/plagioclase mixtures with radiogenic ^{40}Ar contents between 86–97%. VU37-C7 is somewhat heterogeneous (MSWD 1.55), has the lowest K/Ca and an inverse isochron intercept of 325 ± 18 , which is indicative of excess argon. VU37-C8 has a lower MSWD, an isochron intercept equal to 295.5

Fig. 4. Cumulative age probability distribution of $^{40}\text{Ar}/^{39}\text{Ar}$ sanidine ages of the A1 ash layer (A). The area under the curve is proportional to the number of analyses. Individual analyses are plotted with their 1σ analytical errors. The darker shaded area and lighter shaded area represent the analytical weighted standard error and the analytical weighted standard deviation, respectively [15]. The vertical dashed line represents the astronomical age of 6.941 Ma. Three incremental heating spectra of biotite from the A1 (B, C) and SLM3T (D) ash layers are shown. Weighted mean spectrum and isochron ages are also shown including their 1σ analytical errors. Horizontal bars on the right represent astronomical ages of the ash layers. NI: normal isochron; II: inverse isochron.



and is therefore a better age estimate for SL5L. Measurements on SL7L also yield K/Ca ratios characteristic for a sanidine/plagioclase mixture. Combination of the seven analyses of SL7L results in a MSWD of 4.8, indicating potential heterogeneity in the sample. A probability curve indeed shows a non-normal distribution, which can be divided in roughly two populations with about half of the data belonging to one group and the other half to the other (Fig. 5, column A). Therefore, it is difficult to estimate the crystallization age of sanidine for SL7L. Ash layer SL11L yields K/Ca ratios indicative of sanidine and shows an older outlier (xenocrystic contamination?), which has been removed from the dataset. Ages for the older Ptolemais ash layers are 4.973 ± 0.069 Ma for SL11L and 5.094 ± 0.071 Ma for SL5L, respectively.

5.5. The younger Ptolemais ash layers

Pure sanidine separates have been analyzed (most K/Ca > 30) for the five ash layers higher in the stratigraphic succession (Table A1). SLM2T and SR3M both show a few extreme (up to 1 Ma older) outliers, which were omitted from the dataset. SR3M and SR5L then show normal probability distributions in contrast to SLM2T, SLM3T and SR3L. Dividing the data into groups after their irradiation results in more or less two normal distributions (Fig. 5, column A).

Sample inhomogeneity seems not a likely explanation for this bimodality because we have used aliquots of the same separation in various subsequent irradiations as well as newly separated material. Moreover, it is not related to the irradiation itself because the VU32 ages are younger than the VU37 ages for, e.g., SLM3T but older for SLM2T and SR3L. The bimodality may somehow be relat-

Fig. 5. Cumulative probability distributions for $^{40}\text{Ar}/^{39}\text{Ar}$ sanidine ages of Ptolemais ash layers. Extreme outliers are excluded and distributions are separated on the basis of irradiation batch to which the data belong (column A). The x-axis spans in all cases a time interval of 0.5 Ma. Data of [4] have been added to the cumulative probability distributions in column B. The scale on the y-axis is equal for each individual ash layer but is different between ash layers because the area under the curve is proportional to the number of analyses.

ed to short unnoticed departures from the optimal functioning of the analytical system during VU32, despite the fact that both the A1 sanidine as well as the TCR and FCT intercalibrations showed a good reproducibility over several irradiations, including VU32 and VU37. For VU37, non-optimal functioning of the system is less likely because its behavior has been monitored more systematically (e.g., by frequent analyses of mass fractionation, assessment of flat peak shapes) from VU37 onwards. Summarizing, it is not straightforward to select the most reliable age estimates for the Ptolemais tephtras.

Furthermore, most isochron intercepts do not deviate from the atmospheric $^{40}\text{Ar}/^{36}\text{Ar}$ ratio of 295.5 at the 2σ level. Only experiments on SR3L (VU32-C29: 243 ± 14) and SLM3T (VU32-C5: 168 ± 52) significantly deviate from the atmospheric ratio of 295.5. For these ash layers, the VU37 data are considered as more reliable. For the other three upper Ptolemais ash layers, we also preferred the VU37 ages because of the more rigorous monitoring of the analytical system. As a consequence, the resulting ages for SR5L, SR3M, SR3L, SLM3T and SLM2T arrive at 4.196 ± 0.057 , 4.242 ± 0.057 , 4.223 ± 0.057 , 4.301 ± 0.058 and 4.290 ± 0.058 Ma, respectively (Table 1).

Table 1
 $^{40}\text{Ar}/^{39}\text{Ar}$ age and error estimates for Ptolemais and Cretan tephtras and intercalibration with TCR and FCT

	N	MSWD	$R_{\text{tephtra}}^{\text{TC}}$	Error in R		Astr. age (Ma)	Apparent $^{40}\text{Ar}/^{39}\text{Ar}$ age (Ma)				Astronomically calibrated age (Ma)			
				S.E.	S.D.		Age		TCR	FCT	FCT			
							Analytical error	External error						
							S.E.	S.D.	S.E.	S.D.	\pm S.E., \pm S.D.	\pm S.E., \pm S.D.	\pm S.D.	
SR5L	5	0.31	6.7971	0.0171	0.0176	4.280 ± 0.025	4.196	0.011	0.011	0.057	0.057	28.89 ± 0.18 , ± 0.18	28.58 ± 0.18 , ± 0.18	
SR3M	27	0.54	6.7232	0.0046	0.0175	4.318 ± 0.025	4.242	0.003	0.011	0.057	0.058	28.83 ± 0.17 , ± 0.18	28.52 ± 0.17 , ± 0.18	28.61 ± 0.20 MSWD 0.36
SR3L	15	0.22	6.7543	0.0076	0.0133	4.324 ± 0.025	4.223	0.005	0.008	0.057	0.057	29.01 ± 0.17 , ± 0.18	28.69 ± 0.17 , ± 0.18	
SLM3T	15	0.42	6.6313	0.0065	0.0163	4.387 ± 0.025	4.301	0.004	0.011	0.058	0.059	28.89 ± 0.17 , ± 0.18	28.58 ± 0.17 , ± 0.18	
SLM2T	13	0.29	6.6474	0.0066	0.0129	4.408 ± 0.025	4.290	0.004	0.008	0.058	0.058	29.10 ± 0.17 , ± 0.17	28.78 ± 0.17 , ± 0.17	
SL11L	6	0.58	5.7344	0.0180	0.0230	5.015 ± 0.025	4.973	0.016	0.020	0.069	0.070	28.57 ± 0.17 , ± 0.18	28.26 ± 0.17 , ± 0.18	28.28 ± 0.21 MSWD 0.13
SL7L	3	2.85	5.6708	0.0285	0.0720	5.099 ± 0.025	5.028	0.025	0.064	0.072	0.093	28.73 ± 0.20 , ± 0.38	28.41 ± 0.20 , ± 0.38	
SL5L	5	0.26	5.5972	0.0186	0.0194	5.146 ± 0.025	5.094	0.017	0.018	0.071	0.071	28.62 ± 0.17 , ± 0.17	28.30 ± 0.17 , ± 0.17	
A1	95	0.53	4.1346	0.0017	0.0122	6.941 ± 0.025	6.893	0.003	0.020	0.093	0.095	28.53 ± 0.02 , ± 0.09	28.21 ± 0.04 , ± 0.09	

Intercalibration factors $R_{\text{tephtra}}^{\text{TC}}$ between each standard and ash layer are given with the weighted standard error (S.E.) and weighted standard deviation (S.D.). Calculation of the intercalibration factor is described in the text. $R_{\text{tephtra}}^{\text{TC}}$ is used to calculate the $^{40}\text{Ar}/^{39}\text{Ar}$ age, analytical errors and the full external error as outlined in Appendix A. These errors are reported as S.E. and S.D., meaning that either weighted standard errors or weighted standard deviations of $R_{\text{tephtra}}^{\text{TC}}$ are propagated in age and error equations. Furthermore, the $R_{\text{tephtra}}^{\text{TC}}$'s were used to calculate the age of TCR relative to the astronomical age of the ash layer, assuming an uncertainty of 25 kyr in the astronomical age of the Ptolemais ash layers and of 5 kyr for the Cretan A1. Using the intercalibration factor of [17] for TCR and FCT, the age for FCT is calculated relative to the astronomical age of the ash layer as well (see Appendix B). Again, errors reported as S.E. and S.D. mean that either weighted standard errors or weighted standard deviations of $R_{\text{tephtra}}^{\text{TC}}$ are propagated in age and error equations.

The five younger and three older Ptolemais ash layers are combined in two astronomically calibrated FCT ages, respectively. This is done by calculating the weighted mean of all astronomically calibrated FCT ages based on single experiments (i.e., $n = 75$ for the younger and $n = 11$ for the older Ptolemais ash layers) weighted by inverse total variance. The reported error is the ± 1 weighted standard deviation (S.D.). Data for SL7L are reported, but grey and are not included in the combined FCT age because of its unreliable age.

5.6. Ptolemais biotite

$^{40}\text{Ar}/^{39}\text{Ar}$ experiments on biotite have been performed for ash layer SLM3T. The data of VU32-C3 are fusion experiments (4.376 ± 0.062 Ma); VU37-C3 is a stepwise heating experiment resulting in a reliable plateau (4.361 ± 0.061 Ma). The radiogenic ^{40}Ar content varies from 77% to 97% for the steps included in the plateau. Excess argon is not observed because isochron intercepts are all atmospheric at the 2σ level.

6. Discussion

6.1. Previous $^{40}\text{Ar}/^{39}\text{Ar}$ studies on ash layers from Crete and the Ptolemais basin

All ash layers described here have been studied before. Hilgen et al. [3] studied the A1, A2 and A3 ash layers on Crete; Steenbrink (unpublished results) also dated the A1 ash layer and Steenbrink et al. [4] performed $^{40}\text{Ar}/^{39}\text{Ar}$ experiments on the Ptolemais ash layers. In fact, the main reason to extend the $^{40}\text{Ar}/^{39}\text{Ar}$ -astronomical intercalibration studies was the remarkable discrepancy found by [4] between $^{40}\text{Ar}/^{39}\text{Ar}$ and astronomical ages.

The data of [3] are not very consistent, but recalculated ages of [3] (relative to TCR of 28.34 Ma instead of 27.92 Ma as in [3]) are overall older than the data presented here. The biotite ages are total fusion ages, and the assumption of a flat undisturbed age spectrum has not been tested. New biotite analyses were either very heterogeneous to define a reliable incremental heating plateau or reliable plateaus could only be obtained with omission of several steps from the plateau, indicating that the assumption of a flat undisturbed age spectrum by [3] is not met. Apart from biotite, plagioclase has been measured and, for A1, also a sanidine split. As for the new data, it appeared that all analyses on plagioclase in [3] either produced large analytical errors due to the low ^{40}Ar yields, showed heterogeneous populations or isochron intercepts >295.5 , indicative for excess argon. Although five replicate analyses of Faneromeni A1 sanidine are highly reproducible (MSWD 0.28), the isochron intercept is >295.5 . Therefore, the $^{40}\text{Ar}/^{39}\text{Ar}$ data (and conclusions) of [3] must be treated with caution.

The $^{40}\text{Ar}/^{39}\text{Ar}$ data of Ptolemais as published in [4] seem very reliable. MSWD's are low, K/Ca ratios and radiogenic ^{40}Ar yields are high and stepwise heating plateaus of sanidine are excellent. Due to the high radiogenic argon yields, isochron analysis is precluded (clustering of data around the x -axis in inverse isochrons, large error bars in normal isochrons), but slight deviations from the atmospheric ratio for the non-radiogenic argon component will hardly influence the age. Cumulative probability distributions for the VU16 and VU21 data of [4] (recalculated relative to TCR of 28.34 Ma) are plotted in Fig. 5 (column B) together with our VU32 and VU37 data. The VU16 data show younger age peaks, and therefore add another population to the probability distributions. Additionally, the VU16 distributions for SL11L and SLM2T do not display normal distributions. The VU21 data show a multimodal distribution for SL7L, which is also shown in our dataset. The VU21 distribution of SLM2T is equal to the distribution of VU37. For A1, the distribution of the VU21 data of Steenbrink (unpublished results; Fig. 4) is also in agreement with the data presented here. One explanation for the deviation of the VU16 data might be a systematic error in the behavior of the analytical system. As discussed in the previous paragraph, we prefer the VU37 data as the best age estimates, based on more systematic monitoring of the system from VU37 onwards.

6.2. Systematic differences between $^{40}\text{Ar}/^{39}\text{Ar}$ ages and astronomical ages?

Hilgen et al. [3] concluded in their study that $^{40}\text{Ar}/^{39}\text{Ar}$ ages were in good agreement with the astronomical ages. In contrast, [4] noticed a systematic discrepancy of $\sim 3\%$ with $^{40}\text{Ar}/^{39}\text{Ar}$ ages being younger. To solve this inconsistency, all volcanic ash layers were redated. Figs. 4 and 5 unequivocally show that all $^{40}\text{Ar}/^{39}\text{Ar}$ sanidine ages are systematically younger than their astronomical ages, in spite of the occasional lack of clarity about the “real” ages due to multimodal distributions. However, only the analytical uncertainties of sample and standard are incorporated in these figures. To be able to compare the two independent methods, all uncertainties in both methods must be assessed. Error estimates for $^{40}\text{Ar}/^{39}\text{Ar}$ ages must include all uncer-

tainties related to ages of standards and decay constants (e.g., [20]) because we attempt to determine absolute ages. Table 1 shows a list of the $^{40}\text{Ar}/^{39}\text{Ar}$ age estimates including a full error estimate as outlined in Appendix A.

Although Fig. 4 shows that the $^{40}\text{Ar}/^{39}\text{Ar}$ sanidine age for A1 is younger than the astronomical age, the $^{40}\text{Ar}/^{39}\text{Ar}$ age is not statistically different when the so-called full error propagation is applied. This is caused by a proper incorporation of the uncertainties in the activities of the ^{40}K , K and Ar contents in the primary standard and other physical parameters in the error equation. The overall error is not dominated by analytical uncertainties but, as stated before, by the activity of the decay of ^{40}K to ^{40}Ar and the amount of radiogenic ^{40}Ar in the primary standard GA1550. Improvement in the accuracy of the $^{40}\text{Ar}/^{39}\text{Ar}$ ages should therefore be focused on improvements in the accuracy of these two parameters or on a method to avoid or reduce the influence of the two parameters on the final age.

Although the $^{40}\text{Ar}/^{39}\text{Ar}$ ages of the older Ptolemais ashes need to be considered with some caution, that is, SL7L is heterogeneous, and one of the two age populations in SL5L is characterized by excess argon, the remaining $^{40}\text{Ar}/^{39}\text{Ar}$ ages are also younger than their astronomical counterparts (Fig. 5). Full error propagation demonstrates that the statistical significance of this discrepancy is non-existent, as was the case with the A1 data.

The situation for the younger Ptolemais ashes is different. Even when full errors are propagated, the ash layers SLM2T, SLM3T, SR3L, SR3M and SR5L are still significantly younger than the astronomical ages at the 1σ level. Apart from the uncertainties in $^{40}\text{Ar}/^{39}\text{Ar}$ dating which has been accounted for in the error equations, some other possible sources of error might exist. Uncertainties in $^{40}\text{Ar}/^{39}\text{Ar}$ ages can originate from, e.g., contamination during sampling or mineral separation (in this case, with younger crystals), loss of radiogenic ^{40}Ar , biases during mass spectrometry or a combination of these factors. These kinds of systematic errors are difficult to account for. In theory, single crystal analyses might detect possible contamination effects. Unfortunately, most samples have grain sizes which are very small ($<500\ \mu\text{m}$) to allow for reliable single crystal analyses.

On the other hand, an error in the astronomical tuning might also explain the observed difference. The tuning on Crete was straightforward because climate changes related to the orbital parameters are recorded excellently in these marine sediments. Alternative correlations to the target curve showed less consistent patterns, and therefore, the astronomical calibration is assumed to be correct [9]. The few minor misfits may disappear when an improved astronomical solution becomes available. Errors in the astronomical ages for the volcanic ash layers can therefore only be attributed to errors in the astronomical solution itself, uncertainty about the time lag between astronomical forcing, climate response and registration in the stratigraphic record (we assume a zero lag) and the assumption of a constant sedimentation rate between two astronomically calibrated points (i.e., sapropel midpoints). Therefore, we decided to assign an uncertainty of 5 kyr to the astronomical ages of the Cretan tephra (chapter 2 in [18]).

The uncertainties in the tuning of the Ptolemais composite section have been discussed already in [4]. Because of the lack of a clear expression of larger eccentricity-related cycles in Ptolemais, the tuning in Ptolemais is dependent upon a correct magnetostratigraphy, although some of the detailed cycle patterns seem to confirm the tuning of [10]. The astronomical ages for the volcanic ash layers would become older, if the magnetic signal in the Ptolemais section is affected by delayed acquisition [4] and the discrepancy between $^{40}\text{Ar}/^{39}\text{Ar}$ and astronomical ages would even further increase. On the other hand, astronomical ages might be younger, if the effect of delayed acquisition has not been completely eliminated in the Rossello composite and if the magnetostratigraphy of the Ptolemais composite is not affected by delayed acquisition. However, this seems not likely because, in that case, the pattern fit between the sedimentary cycles and insolation curve no longer holds [10], although, in a lacustrine setting, local (tectonic?) processes may play a role. On basis of these uncertainties, we assigned an uncertainty of ~ 25 kyr to the astronomical ages of the ash layers in Ptolemais. Of this 25 kyr, 20 kyr expresses an uncertainty of one cycle in the tuning of the precession-related lignite–marl cycles and 5 kyr expresses the uncertainty for errors in astronomical

solution, lags (or leads?) and interpolation between two calibration points. However, this still leaves the SLM2T, SLM3T, SR3L and SR5L $^{40}\text{Ar}/^{39}\text{Ar}$ ages to be significantly younger.

Furthermore, biotite ages tend to be older than the sanidine ages. Biotite can incorporate excess argon that can rarely be distinguished from radiogenic argon within the mineral, so that anomalously old ages may be obtained [23]. Recoil effects on slightly altered biotite might occur as well (e.g., [24]). But this should be accompanied by clearly increased $^{36}\text{Ar}_{\text{atm}}$ and resultant lower percentages of $^{40}\text{Ar}^*$, which is not observed in our data.

6.3. Intercalibration possibilities between the $^{40}\text{Ar}/^{39}\text{Ar}$ system and astronomical dating?

Sources of systematic error in $^{40}\text{Ar}/^{39}\text{Ar}$ dating are the absolute ages of standards and the exact values of the decay constants. Recent publications focussing on the “true” age of the standards (e.g., [17,21,25,26]) show a range of 27.5–28.5 Ma for the age of the Fish Canyon Tuff. Other publications (e.g., [20,27]) call for improvements in decay constant values. Most of the FCT ages are based on intercalibration to a primary K/Ar dated standard. Min et al. [20] and this study already showed that the final error is dominated by the uncertainty in the activity of the decay of ^{40}K to ^{40}Ar and the uncertainty in the amount of radiogenic ^{40}Ar in the primary standard, if a secondary standard (FCT or TCR) intercalibrated to a primary K/Ar dated standard (GA1550) is used. To reduce the influence of the activity of the ^{40}K decay branch to ^{40}Ar on the final error and to avoid the knowledge of the absolute amount of radiogenic ^{40}Ar in a primary dating standard, the absolute age of a dating standard can be determined by other means (e.g., U/Pb).

Therefore, [20] used the $^{40}\text{Ar}^*/^{39}\text{Ar}_{\text{K}}$ ratios of feldspars from a 1.1 Ga rhyolite and from the 79 AD eruption of the Vesuvius in combination with a Pb/Pb age of the 1.1 Ga rhyolite and the historical age of the eruption of the Vesuvius to determine the age of FCT as a function of the total decay constant. The FCT age calibrated to the 1.1 Ga rhyolite is strongly dependent on the value of the decay constant in contrast to the FCT age calibrated to the 79 AD eruption (see Fig. 9 in [20]). Unfortunately, the analytical precision of this 79

AD eruption is not extremely high due to low amounts of radiogenic ^{40}Ar in such young samples. Kwon et al. [28] combined the data of [20] with three other pairs of $^{40}\text{Ar}^*/^{39}\text{Ar}_{\text{K}}$ ratios and U/Pb reference ages and used a series of statistical methods to infer an FCT age of 28.27 ± 0.07 Ma (and, simultaneously, a total decay constant of $5.476 \pm 0.017 \times 10^{-10} \text{ yr}^{-1}$).

A different approach can be performed with the data presented here. The astronomical age can be considered the “true” age of a volcanic ash layer and the minerals it contains. Table 1 shows a report of the ages for TCR and FCT derived on the basis of astronomical ages of the tephra and their $^{40}\text{Ar}^*/^{39}\text{Ar}_{\text{K}}$ ratios with a most realistic error estimate (see Appendix B for equations). Table 1 shows a report of apparent TCR and FCT ages with both standard errors and standard deviations. In the text, we only mention the standard errors. Fig. 6 visualizes the results from Table 1, including the data for the Vesuvius eruption

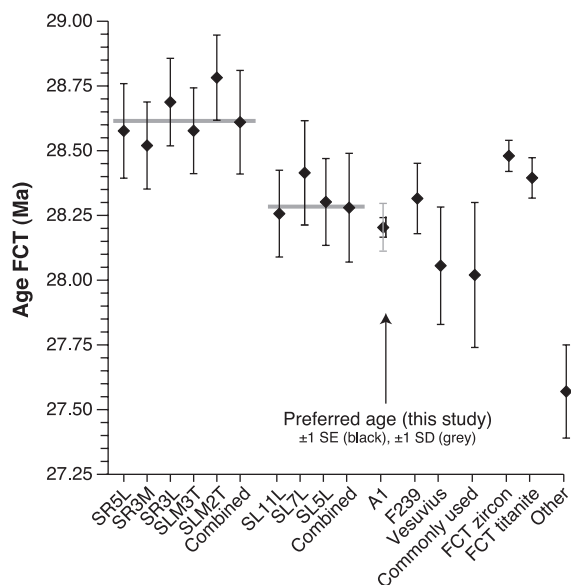


Fig. 6. Age of Fish Canyon Tuff relative to independently dated standards with full error estimate. Astronomically calibrated FCT ages are calculated according to equations in Appendix B. The Ptolemais ash layers are divided in younger and older layers where “combined” represents the weighted average age of the younger and older ash layers, respectively. For comparison, the data of [20] for the Vesuvius and F239 Palisade rhyolite, the commonly used FCT sanidine age of [17], the zircon and titanite ages of [26] and a deviating value (“other”) of [25] are included.

and Palisade rhyolite from [20]. The main advantage of intercalibrating $^{40}\text{Ar}/^{39}\text{Ar}$ dating to astronomically dated standards instead of using FCT or TCR intercalibrated to primary standard GA1550 is that activity data and other physical parameters hardly contribute to the total variance anymore. The reported uncertainty for the age of FCT is now dominated by the analytical errors in the unknowns and standards.

The FCT sanidine age relative to A1 (28.21 ± 0.04 Ma, ± 1 S.E.) shows the most precise age estimate for FCT, even when it is compared to the historical calibrated or U/Pb FC ages (Fig. 6 and Table 1). This is due to a large, consistent $^{40}\text{Ar}/^{39}\text{Ar}$ dataset in combination with an excellent astronomical age control. The data of [20] on the Palisade rhyolite and the Vesuvius eruption support the FCT age based on A1, but uncertainties are higher. The uncertainty in the FCT age relative to U/Pb of the Palisade rhyolite is dominated by the uncertainties in the decay constant and the U/Pb age, the uncertainty in FCT age relative to the 79 AD Vesuvius eruption is dominated by the analytical uncertainty because the exponential nature of radioactive decay results in low amounts of $^{40}\text{Ar}^*$ in sanidine of the 79 AD Vesuvius eruption. Furthermore, this age is in excellent agreement with the 28.27 ± 0.07 Ma of [28].

The older Ptolemais ashes are consistent with the FCT age relative to A1, although uncertainties are higher partly due to the higher uncertainty (± 25 kyr) assigned to the astronomical ages for ash layers in Ptolemais. The older Ptolemais ashes yielded a combined age of 28.28 ± 0.21 Ma for FCT. The younger Ptolemais ashes produce an older age for FCT and combination of the five younger Ptolemais volcanic ash layers result in an age of 28.61 ± 0.20 Ma. Although the $^{40}\text{Ar}/^{39}\text{Ar}$ ages might be subject to sources of error as discussed in the previous paragraph, an error in the astronomical tuning can not be excluded for Ptolemais. The older and younger Ptolemais ash layers are separated by a stratigraphic interval that might contain a hiatus. Consequently, a possible error in the tuning might not be identical for the lower and upper parts of the Ptolemais Formation in which the two clusters of ash layers occur. But this error will most likely be the same for ash layers in either of the two clusters because they are found in parts of the Ptolemais Formation in which the undisturbed succession of successive individual precession related cycles

is evident. We are inclined to assume that the accordance between A1, Palisade rhyolite, 79 AD Vesuvius and the older Ptolemais ashes points to an erroneous tuning for the younger Ptolemais ashes and that the apparent FCT age of 28.61 ± 0.20 Ma relative to younger Ptolemais ashes is by coincidence consistent with the U/Pb zircon concordia age (28.48 ± 0.06 Ma) for FCT zircon [26]. The U/Pb age of FCT might be a high estimate for the time of the eruption because it may include a component of pre-eruptive residence time. Residence times of 300 kyr are well documented but become proportionally insignificant for older U/Pb data as used by [28], and thus will not introduce a significant bias in their results.

Ideally, more research, preferably single crystal sanidine dating of ash layers intercalated in other well-tuned marine sections, is required to support the age of FCT relative to the Cretan and older Ptolemais astronomically dated ash layers (and that tuning in the younger part of the Ptolemais section is wrong). When the implicit assumptions in this intercalibration approach are true (e.g., negligible time span between closure of the mineral for argon diffusion—moment of eruption—and deposition in the sediments, no xenocrystic contamination, no argon loss from samples, correct astronomical tuning), we expect to see the same systematic differences between both methods, and intercalibration must result in the same age for FCT.

7. Conclusions

$^{40}\text{Ar}/^{39}\text{Ar}$ sanidine ages of volcanic ash layers tend to be younger than astronomical ages. However, when a more realistic error propagation method is used, the discrepancy statistically disappears for part of the ash layers (A1 and older Ptolemais ashes). Unfortunately, errors in $^{40}\text{Ar}/^{39}\text{Ar}$ ages increase from $\sim 0.3\%$ to 1.3% when the improved full error propagation method is used. This increase is attributed to uncertainties in the absolute age of standards and parameters related to the decay constants. The few biotite ages tend to be older than the sanidine ages, which might be caused by the combined effects of excess argon (although not observed in isochrons due to clustering of data, and therefore higher uncertainties) and recoil processes.

To circumvent the increase in error due to applying more realistic error approaches, we intercalibrated two commonly used standards (TCR/FCT) with the $^{40}\text{Ar}^*/^{39}\text{Ar}_K$ ratios of the astronomically dated ash layers. It appeared that the uncertainty in the newly derived ages for FCT was dominated by analytical errors only for A1 and analytical errors and uncertainties in the astronomical ages for Ptolemais. The new ages for TCR/FCT are 28.53 ± 0.02 (0.09)/ 28.21 ± 0.04 (0.09) Ma (± 1 S.E. and between brackets, ± 1 S.D.), respectively, based on A1 and supported by the older Ptolemais ash layers and data published in Refs. [20,28]. The intercalibration of FCT with the younger Ptolemais ashes results in an age of 28.61 ± 0.20 Ma. The difference with the previous data is most likely due to an error in the tuning of the upper part of the Ptolemais section. However, ideally, more research should confirm this tuning error, as the proposed FC age relative to A1 should be confirmed by other direct astronomically dated ash layers.

8. References cited in the Appendix

[30–33]

Acknowledgements

Al Deino is acknowledged for his contributions in the field. We thank Jaime Dinares-Turell, Paul Renne and an anonymous reviewer for their useful contributions. Mineral preparation facilities were provided by R. van Elsas, Vrije Universiteit Amsterdam. This project is part of the research program of the Netherlands School for Sedimentary Geology (NSG) and is financially supported by ALW grant 75019802 to K.K. The Netherlands Research Centre for Integrated Solid Earth Science (ISES) financially contributed to fieldwork expenses of F.H. and J.W. [BARD]

References

- [1] L.J. Lourens, F.J. Hilgen, J. Laskar, N.J. Shackleton, D. Wilson, The Neogene period, in: F. Gradstein, J. Ogg, A. Smith (Eds.), A Geological Timescale, Cambridge University Press, 2004.
- [2] P.R. Renne, A.L. Deino, R.C. Walter, B.D. Turrin, C.C. Swisher, T.A. Becker, G.H. Curtis, W.D. Sharp, A.-R. Jaouni, Intercalibration of astronomical and radioisotopic time, *Geology* 22 (1994) 783–786.
- [3] F.J. Hilgen, W. Krijgsman, J.R. Wijbrans, Direct comparison of astronomical and $^{40}\text{Ar}/^{39}\text{Ar}$ ages of ash beds: potential implications for the age of mineral dating standards, *Geophysical Research Letters* 24 (1997) 2043–2046.
- [4] J. Steenbrink, N. Van Vugt, F.J. Hilgen, J.R. Wijbrans, J.E. Meulenkamp, Sedimentary cycles and volcanic ash beds in the lower Pliocene lacustrine succession of Ptolemais (NW Greece): discrepancy between $^{40}\text{Ar}/^{39}\text{Ar}$ and astronomical ages, *Palaeogeography, Palaeoclimatology, Palaeoecology* 152 (1999) 283–303.
- [5] S.B. Pavlides, D.M. Mountrakis, Extensional tectonics of northwestern Macedonia, Greece, since the late Miocene, *Journal of Structural Geology* 9 (1987) 385–392.
- [6] G. Marakis, C. Sideris, Petrology of the Edessa area volcanic rocks, western Macedonia, Greece, *Bulletin Volcanologique* 36 (1973) 462–472.
- [7] N. Kolios, F. Innocenti, P. Manetti, A. Peccerillo, O. Giuliani, The Pliocene volcanism of the Voras Mts. (central Macedonia, Greece), *Bulletin Volcanologique* 43 (1980) 553–568.
- [8] W. Krijgsman, F.J. Hilgen, C.G. Langereis, A. Santarelli, W.J. Zachariasse, Late Miocene magnetostratigraphy, biostratigraphy and cyclostratigraphy in the Mediterranean, *Earth and Planetary Science Letters* 136 (1995) 475–494.
- [9] F.J. Hilgen, W. Krijgsman, C.G. Langereis, L.J. Lourens, A. Santarelli, W.J. Zachariasse, Extending the astronomical (polarity) time scale into the Miocene, *Earth and Planetary Science Letters* 136 (1995) 495–510.
- [10] N. van Vugt, J. Steenbrink, C.G. Langereis, F.J. Hilgen, J.E. Meulenkamp, Magnetostratigraphy-based astronomical tuning of the early Pliocene lacustrine sediments of Ptolemais (NW Greece) and bed-to-bed correlation with the marine record, *Earth and Planetary Science Letters* 164 (1998) 535–551.
- [11] J. Laskar, F. Joutel, F. Boudin, Orbital, precessional, and insolation quantities for the Earth from -20 Myr to $+10$ Myr, *Astronomy and Astrophysics* 270 (1993) 522–533.
- [12] F.J. Hilgen, Extension of the astronomically calibrated (polarity) time scale to the Miocene/Pliocene boundary, *Earth and Planetary Science Letters* 107 (1991) 349–368.
- [13] L.J. Lourens, A. Antonarakou, F.J. Hilgen, A.A.M. Van Hoof, C. Vergnaud-Grazzini, W.J. Zachariasse, Evaluation of the Plio–Pleistocene astronomical timescale, *Paleoceanography* 11 (1996) 391–413.
- [14] A.A.P. Koppers, ArArCALC-software for $^{40}\text{Ar}/^{39}\text{Ar}$ age calculations, *Computers & Geosciences* 28 (2002) 605–619.
- [15] J.R. Taylor, An Introduction to Error Analysis, The Study of Uncertainties in Physical Measurements, University Science Books, Sausalite, CA, 1997, 327 pp.
- [16] I. Wendt, C. Carl, The statistical distribution of the mean squared weighted deviation, *Chemical Geology. Isotope Geoscience Section* 86 (1991) 275–285.
- [17] P.R. Renne, C.C. Swisher, A.L. Deino, D.B. Karner, T.L. Owens, D.J. DePaolo, Intercalibration of standards, abso-

- lute ages and uncertainties in $^{40}\text{Ar}/^{39}\text{Ar}$ dating, *Chemical Geology* 145 (1998) 117–152.
- [18] K.F. Kuiper, Direct intercalibration of radio-isotopic and astronomical time in the Mediterranean Neogene, *Geologica Ultraiectina* 235, PhD thesis, Utrecht University, 2003.
- [19] R.H. Steiger, E. Jäger, Subcommission on geochemistry: convention on the use of decay constants in geo- and cosmochronology, *Earth and Planetary Science Letters* 36 (1977) 359–362.
- [20] K. Min, R. Mundil, P.R. Renne, K.R. Ludwig, A test for systematic errors in $^{40}\text{Ar}/^{39}\text{Ar}$ geochronology through comparison with U/Pb analysis of a 1.1-Ga rhyolite, *Geochimica et Cosmochimica Acta* 64 (2000) 73–98.
- [21] T.L. Spell, I. McDougall, Characterization and calibration of $^{40}\text{Ar}/^{39}\text{Ar}$ dating standards, *Chemical Geology* 198 (2003) 189–211.
- [22] R.J. Fleck, J.F. Sutter, D.H. Elliot, Interpretation of discordant $^{40}\text{Ar}/^{39}\text{Ar}$ age-spectra of Mesozoic tholeiites from Antarctica, *Geochimica et Cosmochimica Acta* 41 (1977) 15–32.
- [23] I. McDougall, M.T. Harrison, *Geochronology and Thermochronology by the $^{40}\text{Ar}/^{39}\text{Ar}$ Method*, Oxford Univ. Press, New York, 1999, 269 pp.
- [24] K. Min, P.R. Renne, W.D. Huff, $^{40}\text{Ar}/^{39}\text{Ar}$ dating of Ordovician K-bentonites in Laurentia and Baltoscandia, *Earth and Planetary Science Letters* 185 (2001) 121–134.
- [25] M.A. Lanphere, H. Baadsgaard, Precise K–Ar, $^{40}\text{Ar}/^{39}\text{Ar}$, Rb–Sr and U/Pb mineral ages from the 27.5 Ma Fish Canyon Tuff reference standard, *Chemical Geology* 175 (2001) 653–671.
- [26] M.D. Schmitz, S.A. Bowring, U–Pb zircon and titanite systematics of the Fish Canyon Tuff; an assessment of high-precision U–Pb geochronology and its application to young volcanic rocks, *Geochimica et Cosmochimica Acta* 65 (2001) 2571–2587.
- [27] F. Begemann, K.R. Ludwig, G.W. Lugmair, K. Min, L.E. Nyquist, P.J. Patchett, P.R. Renne, C.-Y. Shih, I.M. Villa, R.J. Walker, Call for an improved set of decay constants for geochronological use, *Geochimica et Cosmochimica Acta* 65 (2001) 111–121.
- [28] J. Kwon, K. Min, P. Bickel, P.R. Renne, Statistical methods for jointly estimating decay constant of ^{40}K and age of a dating standard, *Mathematical Geology* 34 (2002) 457–474.
- [29] M. Fytikas, F. Innocenti, P. Manetti, R. Mazzuoli, A. Peccerillo, L. Villari, Tertiary to Quaternary evolution of volcanism in the Aegean region, in: J.E. Dixon, A.H.F. Robertson (Eds.), *The Geological Evolution of the Eastern Mediterranean*, Special Publication-Geological Society London, vol. 17, 1984, pp. 687–699.
- [30] E.L. Garner, T.J. Murphy, J.W. Gramlich, P.J. Paulsen, I.L. Barnes, Absolute isotopic abundance ratios and the atomic weight of a reference sample of potassium, *Journal of Research of the National Bureau of Standards* 79A (1975) 713–725.
- [31] E.R. Cohen, B.N. Taylor, The 1986 CODATA recommended values of the fundamental physical constants, *Journal of Research of the National Bureau of Standards* 92 (1987) 85–95.
- [32] R.D. Beckinsale, N.H. Gale, A reappraisal of the decay constants and branching ratio of ^{40}K , *Earth and Planetary Science Letters* 6 (1969) 289–294.
- [33] I. McDougall, Z. Roksandic, Total fusion $^{40}\text{Ar}/^{39}\text{Ar}$ ages using HIFAR reactor, *Journal of the Geological Society of Australia* 21 (Part 1) (1974) 81–89.